Non-Ideality by Sedimentation Velocity of Halophilic Malate Dehydrogenase in Complex Solvents

Alexandra Solovyova,*† Peter Schuck,‡ Lionel Costenaro,* and Christine Ebel*
*Laboratoire de Biophysique Moléculaire, Institut de Biologie Structurale J. P. Ebel, F-38027 Grenoble, France; †Institute for Problems of Cryobiology and Cryomedicine of the National Academy of Sciences of Ukraine, 61015 Kharkov, Ukraine; and ‡Division of Bioengineering and Physical Science, Office of Research Services, National Institutes of Health, Bethesda, Maryland 20892 USA

ABSTRACT We have investigated the potential of sedimentation velocity analytical ultracentrifugation for the measurement of the second virial coefficients of proteins, with the goal of developing a method that allows efficient screening of different solvent conditions. This may be useful for the study of protein crystallization. Macromolecular concentration distributions were modeled using the Lamm equation with the approximation of linear concentration dependencies of the diffusion constant, $D = D^\circ (1 + k_D c)$, and the reciprocal sedimentation coefficient $s = s^\circ/(1 + k_s c)$. We have studied model distributions for their information content with respect to the particle and its non-ideal behavior, developed a strategy for their analysis by direct boundary modeling, and applied it to data from sedimentation velocity experiments on halophilic malate dehydrogenase in complex aqueous solvents containing sodium chloride and 2-methyl-2,4-pentanediol, including conditions near phase separation. Using global modeling for three sets of data obtained at three different protein concentrations, very good estimates for k_s and s° and also for D° and the buoyant molar mass were obtained. It was also possible to obtain good estimates for k_D and the second virial coefficients. Modeling of sedimentation velocity profiles with the non-ideal Lamm equation appears as a good technique to investigate weak inter-particle interactions in complex solvents and also to extrapolate the ideal behavior of the particle.

INTRODUCTION

The behavior of macromolecules is termed as ideal in very dilute solutions. In this limit, their positions, orientations, and movements are considered to be non-correlated. The macroscopically measured quantities usually are averages over an ensemble of molecules but nevertheless reflect the properties of individual particles, for example, molar mass and dimensions. In real solutions, however, even weak inter-particle interactions will cause a concentration dependence of the observed properties. Free-particle properties are obtained, therefore, from extrapolation of the data to infinite dilution of the macromolecule, and their concentration dependencies provide information about inter-particle interactions. In the past, the study of such weak inter-particle interactions has been the object of numerous studies because of its practical importance in many processes involving colloids in industry (e.g., paints, foods, and cosmetics). For example, weak interactions determine the tendency for a suspension of particles to remain in solution, to aggregate, to overcome phase separation or to form crystals. Interest has focused more recently on biological macromolecules in concentrated solution, with the aim of understanding their capacity to form crystals, which still represents a crucial and frequently very difficult step for the determination of their three-dimensional structure at high resolution. Likewise, studies on biological macromolecules in concentrated solutions are stimulated by the increasing awareness of the effect of macromolecular crowding on the biological function, for example, of proteins in the cytosol of a cell.

The static and transport properties of macromolecules in solution are related not only to the particle characteristics but also to their spatial distribution, which depends on intermolecular interactions (Pusey and Tough, 1985). The entire inter-particle interactions in solution determine the value of the second virial coefficient A_2, which has positive values for globally repulsive inter-particle interactions and negative values in the case of global attraction. Restricting the consideration to quasi-spherical particles, the second virial coefficient is related to the pair correlation function $g(r)$, which expresses the probability of finding particles of molar mass M at a distance r:

$$A_2 = 2\pi N_A/M^2 \int (1 - g(r))r^2 dr$$

For weakly interacting spheres, the pair correlation function $g(r)$ can be related, in terms of MacMillan-Mayer theory, to the mean particle-particle interaction potential $W(r)$ (MacMillan and Mayer, 1945):

$$g(r) = \exp^{-W(r)/kT}$$

The spatial particle distribution modulates the elastic scattering of the macromolecule in solution. Because $g(r)$ can be extracted from scattering profiles and calculated from pair potentials (Belloni, 1991), scattering techniques have been used to model inter-macromolecular potentials (Malfois et

Received for publication 27 November 2000 and in final form 18 June 2001.

Address reprint requests to Dr. Christine Ebel, Laboratoire de Biophysique Moléculaire, Institut de Biologie Structurale J. P. Ebel, UMR 5075 CEA-CNRS-UJF, 41, rue Jules Horowitz, F-38027 Grenoble Cedex 01, France. Tel.: 33-0-4-38789638; Fax: 33-0-4-38785494; E-mail address: christine.ebel@ibs.fr.

0006-3495/01/10/1868/13 $2.00

al., 1996). Furthermore, the spatial and velocity correlations between particles in solution also determine the dynamic properties of the macromolecules in solution, for example, the collective diffusion coefficient and its concentration dependency as well as the concentration dependence of the friction coefficient. Different theoretical approaches have been described for the concentration dependencies of the friction and diffusion coefficients of diluted hard spheres, interacting through excluded volume effects, Coulomb repulsion, and van der Waals attraction (see references in Pusey and Tough, 1985). In another approach, the role of shape and solvation is emphasized (Rowe, 1992; Harding and Johnson, 1985a). As indicated above, there is a recent renewed interest in the measurement of parameters related to non-ideality. For a number of proteins in solvents known to promote crystallization, A_2 values measured in undersaturated or supersaturated solutions are moderately negative and lie in a fairly narrow range, and an experimental relationship with protein solubility has been established (George and Wilson, 1994; George et al., 1997; Guo et al., 1999; Bonneté et al., 1999).

Halophilic malate dehydrogenase from *Haloarcula marismortui* (*Hm* MalDH) is being studied in our laboratory as a model protein for the effect of the environment on protein folding, stability, solubility, and dynamics. The bacteria grow in media that are nearly saturated with salt, mainly sodium chloride, and their cytoplasm is also nearly saturated with salt, mainly potassium chloride. Halophilic proteins have a high content of acidic amino acid residues, which is related to their instability in the absence of high salt concentrations. Ions of high charge density are the most efficient for stabilizing the protein at low salt (Ebel et al., 1999a). Anion binding was observed on the very acidic protein through high-resolution structure determination by x-ray crystallography (Richard et al., 2000), and salt binding was inferred from solvation studies performed in NaCl and KCl by various complementary methods (Bonneté et al., 1993; Kernel et al., 1999). Recent results showed that the solvation is very different for different salts (Ebel et al., 1998; C. Ebel, M. Pascu, P. Faou, L. Costenaro, G. Zaccai, in preparation). The weak inter-particle interactions in various salts were characterized by measurements of the second virial coefficients (Ebel et al., 1999b). Conditions of high protein solubility were in general, but not always, associated with positive values of A_2. Values for the second virial coefficient decrease slightly with increasing salt concentration, and values close to zero or negative values were associated with precipitation or crystallization conditions. The best crystals are found after a complex dilution process initiated in a biphasic drop in the presence of 2-methyl-2,4-pentanediol (MPD) and NaCl (Richard et al., 1995; Dym et al., 1995). Previously, we have determined the solvent composition in the environment of the protein during the dilution process of the crystallization drop. By measuring the second virial coefficient by neutron scattering, we have found that crystal formation is correlated with a slow evolution from repulsive to attractive protein-protein interactions (Costenaro et al., 2001). Based on the hypothesis that such an evolution may be promoting crystallization more generally, our aim is now to define the determinants of this behavior.

For this purpose, before a more detailed analysis, it would be very useful to be able to rapidly screen a variety of solvents containing high concentrations of inorganic and organic solutes for their effect on the second virial coefficient. The second virial coefficient can be evaluated from a variety of measurements, which are those able to provide the molar mass in a rigorous way (Eisenberg, 1976, 1981). Among these techniques, many have drawbacks in practice. For example, precise osmotic pressure measurements are very difficult to perform in solvents concentrated in salt, light scattering is very sensitive to sample heterogeneity, and neutron or x-ray scattering experiments require large instrument facilities. Sedimentation equilibrium analytical ultracentrifugation suffers from the requirement that in the presence of salts or organic solvents at high concentrations, due to preferential interactions of the protein with solvent components, the buoyant molar mass (and often also a baseline parameter) needs to be determined from the experiment simultaneously together with the second virial coefficient; this makes a precise determination of A_2 difficult. As an alternative ultracentrifugal method, A_2 can be determined, in theory, from the concentration dependence of the sedimentation and diffusion coefficients, both of which determine the shape of sedimentation boundary profiles in velocity ultracentrifugation. It has been shown that the sedimentation profiles are very sensitive to weak interparticle interactions, most notably through the concentration dependency of s. In particular, repulsive interactions produce retardation and sharpening of the sedimentation profiles, as studied in detail by Yphantis and co-workers (Dishon et al. 1967; Fujita, 1975) and others, and a large literature exists on different traditional and more recent descriptions and methods for their analysis (Fujita. 1975; Dishon et al. 1967; van Holde and Weischet 1978; Behlke and Ristau, 1997; Demeler and Saber, 1998).

In the present study, we have investigated whether weak inter-particle interactions and the second virial coefficient could be evaluated from sedimentation velocity experiments. To allow for a large concentration range, we used the Rayleigh interference optical detection and applied direct boundary modeling by Lamm equation solutions (Schuck, 1998), modified to take into account linear dependencies (k_D and k_s) for D and $1/s$, and algebraic systematic noise decomposition (Schuck and Demeler, 1999). First, simulated curves were used to validate a fitting procedure of the parameters characterizing the particle and its non-ideal behavior. Then, the fitting procedure was applied to experimental sedimentation velocity experiments performed on halophilic malate dehydrogenase at different protein con-

centrations. By using samples of only 105 μl, the total amount of protein was less than 2 mg for each of the three solvent conditions studied. The results were compared with those obtained by dynamic light scattering and small-angle neutron-scattering techniques.

EXPERIMENTAL PROCEDURES AND THEORETICAL BACKGROUND

Preparation of the protein and solvents

Hm MalDH was over-expressed in *Escherichia coli* and purified as previously described (Cendrin et al., 1993), with a final step of gel filtration in 4 M NaCl, and stored as a concentrated sample in this solvent at 4°C. The solutions of *Hm* MalDH in MPD and NaCl were prepared by dialysis before the sedimentation experiments or by weight dilutions followed by ultracentrifugation for a few minutes at 175,000 × *g* for the light-scattering experiments, respectively (these experiments were not performed at constant chemical potential of the solvent components but the difference in *D*-values should be very small). All solvents are buffered with Tris-HCl 50 mM, pH 8. Protein concentration was measured in an UV spectrometer using an extinction coefficient at 280 nm of 0.85 $cm^2\ mg^{-1}$. Density measurements of the solvents were performed using a DMA-58 device (Anton PAAR, Graz, Austria).

Sedimentation velocity experiments and numerical procedure of boundary modeling

The sedimentation velocity experiments were carried out in an analytical ultracentrifuge Optima XLA-I (Beckman, Palo Alto, CA), using a four-hole rotor AN-Ti at rotor speeds of 42,000 rpm or 60,000 rpm and at a temperature of 20°C. We used interference optics for the detection of the protein concentration as a function of radial position and time. The *Hm* MalDH and solvent solutions (105 μl) were filled in 3-mm double-sector centerpieces. (In these cells, the total number of fringes is approximately equal to the loading concentration expressed in mg/ml.) In a second set of experiments, ~300 μl of solution was filled in 12-mm double-sector centerpieces. One hundred acquisitions were performed in intervals of 4–5 min. The calculated loading concentrations measured in fringe units resulting from the data analysis were used to convert k_s and k_D from fringe units into mass units.

Theoretical concentration distributions were calculated by finite element solutions of the Lamm equation (Eq. 4 below) with static or moving frame of reference, as described by Claverie (1976) and Schuck (1998), respectively. The concentration dependence of $s(c)$ and $D(c)$ (Eqs. 8 and 9 below) was introduced locally in each time-step, applying a two-step propagation scheme for improved accuracy (Schuck, 1998). We implemented separately the cases for repulsive ($k_s > 0$, $k_D > 0$) and attractive ($k_s < 0$, $k_D < 0$) interactions. The calculated profiles were compared with those described in the literature (Dishon et al., 1967). It was verified that they exhibit the typical sharpening and retardation and that they approach a time-independent boundary shape in highly non-ideal conditions. Furthermore, as a test for their numerical accuracy we applied the transformation of $[\ln(c/c_0) - (1 + k_s c_p) \times \ln(c_p - c/c_0)]$ versus r^2 (for the case of $k_D = 0$). As described by Yphantis and colleagues, for concentration-dependent sedimentation of the form $s(c) = s°/(1 + k_s c)$, this function transforms the theoretically expected (limiting) steady-state boundary shapes into straight lines with slopes equal to $(0.5\omega^2 s°/D°)[k_s c_p/(1 + k_s c_p)]$. As expected, with increasing non-ideality, the transformed boundaries approached straight lines with slopes close to the theoretical value, although at slightly lower precision than as described in Dishon et al. (1967). For the analysis of experimental profiles, a number of data transformation approaches have been developed previously (Dishon et al., 1967; Fujita, 1975). However, we took advantage of the rapid calculation of numerical solutions and employed direct nonlinear regression of the raw data (see below). Systematic noise components in the interference optical data were calculated algebraically as described previously (Schuck and Demeler, 1999). This approach was incorporated into the software SEDFIT, which is available from the authors on request.

For global modeling, an extended version of SEDFIT was used that provides for several data channels, each containing a series of scans of a sedimentation velocity experiment. For global regression, all experiments were given equal weights. The loading concentrations and the systematic noise parameters were optimized locally to each data channel, whereas $s°$, $D°$, k_s, and k_D were optimized globally.

Dynamic light-scattering experiments

Dynamic light-scattering (DLS) was performed using a DynaPro-801 Instrument (Protein Solutions, Charlottesville, VA) and analyzed using the provided Autopro software. A volume of 7 μl was illuminated at λ = 780 nm by a 25-mW solid-state laser, and the auto-correlation function of the light intensity scattered at θ = 90° was measured for 3.3 ms in intervals of ~4 μs. The normalized auto-correlation functions $R(t)$ from typically three sets of ~25 measurements were averaged and analyzed in terms of one or two exponential decays of amplitude c_i and decay constant τ_i, and a baseline b:

$$R(t) = b + \sum c_i e^{t/\tau_i} \tag{1}$$

The diffusion coefficients D_i are calculated from the values of the decay constant:

$$D_i = \tau_i / q^2 \tag{2}$$

where q denotes the scattering vector $q = (4\pi/\lambda) \times n \times \sin(\theta/2)$ with the refractive index n. To correct for the temperature effects, the diffusion coefficients D_{20} were calculated considering the temperature dependency of the viscosity η:

$$D_{20} = D/(293.15/T)(\eta/\eta_{20}), \tag{3}$$

with T denoting the temperature of the solution in Kelvin. Tabulated values for the viscosity and refractive index for water were used.

Theoretical background

The Lamm equation expresses the spatial and temporal evolution of the concentration c of a homogeneous solute in the centrifugal field as a function of its sedimentation and diffusion coefficients (s and D) (Lamm, 1929; Tanford, 1961):

$$\partial c/\partial t = 1/r\partial[(D\partial c/\partial r - cs\omega^2 r)r]/\partial r, \tag{4}$$

with t denoting the time, r the distance to the axis of rotation, and ω the angular velocity. The sedimentation coefficient s is related to the buoyant molar mass $M(\partial\rho/\partial c)_{T,\mu}$, and to the friction coefficient f, through the Svedberg equation (Svedberg and Pederson, 1940):

$$s = M(\partial\rho/\partial c)_{T,\mu_S}/N_A f \tag{5}$$

In this expression, N_A is the Avogadro number, and $(\partial\rho/\partial c)_{T,\mu S}$ is the increment of the solution density ρ at constant temperature T and chemical potential μ_S of solvent components, c the protein concentration in mass unit, and M its molar mass. The increment of density is $(1 - \rho^0 \bar{V})$ in one-component solvents, with ρ^0 denoting the solvent density and $\bar{V}$ the partial specific volume of the macromolecule (Eisenberg, 1976). For an incompressible fluid, the Stokes-Einstein relation

$$D = (\partial\Pi/\partial C)_{T,\mu_S}/N_A f \quad (6)$$

(Pusey and Tough, 1985; Schmitz, 1990; Harding and Johnson, 1985a) relates the diffusion coefficient D to the friction coefficient f and the osmotic susceptibility $(\partial\Pi/\partial C)_{T,\mu_S}$ (C denoting the solute concentration in molar units). The osmotic susceptibility can be related to the chemical potential μ of the macromolecule through the identity $(\partial\Pi/\partial C)_{T,\mu S} = c(\partial\mu/\partial c)_{T,\mu_S}$ and approaches RT in the limit of infinite dilution. In this limit, the diffusion coefficient is $D^\circ = RT/N_A f^\circ$, where R is the gas constant, and the friction coefficient can be calculated via the hydrodynamic radius, R_H, as $f^\circ = 6\pi\eta R_H$. Accordingly, f° is related to the mean size and the shape of the macromolecule. The buoyant molar mass can be obtained from the combination of s° and D°:

$$s^\circ/D^\circ = (\partial\rho/\partial c)_{T,\mu_S} M/RT \quad (7)$$

In non-ideal solutions, the macromolecule concentration influences s and D through spatial and velocity correlations between particles. For moderate protein concentrations, s, D, and f can be described in the linear approximations:

$$s/s^\circ = f^\circ/f = (1\text{-}k'_s c + \cdots) = 1/(1 + k_S c + \cdots), \quad (8)$$

$$D/D^\circ = (1 + k_D c + \cdots) \quad (9)$$

At not too high protein concentrations, both variants of Eq. 8 are very similar, and $k_s \approx k'_s$. (An alternative formulation on the basis of $s_{w,20}$ and $D_{w,20}$ values, which explicitly contains terms involving partial specific volumes has been discussed by Harding and Johnson (1985a).) Both k_s and k_D can be either positive or negative, with positive values corresponding to conditions of repulsive interactions and negative values to attractive interactions. The osmotic susceptibility $(\partial\Pi/\partial C)_{T,\mu_S}$ can be expanded in power series of the concentration and related to the second virial coefficient A_2 expressed in ml mol g^{-2}:

$$(\partial\Pi/\partial C)_{T,\mu_S} = RT(1 + 2A_2 Mc + \cdots) \quad (10)$$

It should be noted that A_2 is here the same second virial coefficient that can be obtained from the concentration dependence of the apparent molar mass M_{app} in equilibrium sedimentation or in scattering techniques via the relationship $1/M_{app} = 1/M + 2\,A_2 c + \ldots$. Inserting Eqs. 10 and 8 into 6 and comparison of the terms linear in concentration with Eq. 9 leads to

$$k_D \approx 2A_2 M - k_s \approx 2A_2 M - k'_s. \quad (11)$$

This relationship allows the calculation of the second virial coefficient from k_s and k_D. Inspection of Eq. 11 shows two sources of non-ideality determining the values of k_D: thermodynamic non-ideality, which is related to A_2 and leads to the concentration dependency of the molar mass, and hydrodynamic non-ideality, which is related to that of the frictional coefficient and of the sedimentation coefficient. Because it is the difference between two numbers of the same sign and of similar magnitudes (which is expected if A_2 and k_S are linked to the weak inter-particle interactions), k_D can be expected to be smaller than $2A_2M$ or k_S. Further, in general, k_D, k_S, and $2A_2M$ should have the same sign (theoretical exceptions correspond to small values of A_2, with a mixture of attractive and repulsive interactions (Pusey and Tough, 1985)).

RESULTS AND DISCUSSION

Modeling the effect of non-ideality on the sedimentation boundary

A large number of laboratories have studied the effects of concentration dependence of s on the sedimentation profiles; fewer have considered concentration dependence of D. In the present context, we have reexamined the influence of k_s and k_D on the sedimentation profiles to evaluate their relative contributions to deviations from ideal boundaries and to study the inverse problem if parameter values can be extracted by direct boundary modeling of noisy data.

First, we consider a boundary localized nearly in the middle of the centrifuge cell for a solute that is characterized by $s^\circ = 2.5$ S and $D^\circ = 2.5 \times 10^{-7}$ cm^2 s^{-1}, at a concentration of 10 mg/ml and in the absence of concentration dependence of D. In Fig. 1, *A* and *B*, simulated sedimentation profiles and their radial derivatives are compared, in the ideal case ($k_s = 0$, solid line) or with a k_s value of 10 ml/g (dotted line), which grossly corresponds to our experimental values for the repulsive case (see below). The well-known retardation of the boundary associated to its sharpening is apparent, and opposite effects are observed in the case of attractive interactions corresponding to negative values of k_s (data not shown). It is obvious that extracting a D value from the boundary spreading of concentration-dependent sedimentation profiles without taking into account the inter-particle effects would lead to an incorrect description of the macromolecule. Second, we have studied the effect of k_D on the sedimentation boundaries. As can be seen in Fig. 1 *C*, in a 3-mm cell at protein loading concentrations of >10 mg/ml, the effect of k_D values >1 ml/g already exceeds the instrumental noise. However, in real experiments, we would expect significantly affected boundaries only when k_D is greater than 3 ml/g. The deformations due to the concentration dependence of D is exaggerated in the derivative curve of Fig. 1 *D*, by using a k_D value of 100 ml/g, which is one to two orders of magnitude larger than the values to be expected under most experimental conditions. In this case, we observe a significant deviation of the gradient curve from the Gaussian shape, combined with a slight displacement of its maximum value. For negative k_D values corresponding to attractive conditions, sharpening of the boundary is observed (data not shown).

The inspection of these simulated data suggests that s° and k_s values should be easily extracted, even from a single sedimentation velocity experiment, whereas fits of D° and k_D may be more difficult. Because a global nonlinear regression of several sedimentation velocity experiments is very computationally intensive and difficult to initialize, we studied first how much information can be extracted from single-experiment analyses. We simulated a series of concentration distributions of non-ideal sedimentation with $s^\circ = 2$ S, $D^\circ = 1.5 \times 10^{-7}$ cm^2 s^{-1}, combining concentration dependencies of s and D, with $|k_s| = |k_D| = 12.5$ ml/g, and introduced statistical noise of 0.01 fringes. The s° and D° values are close to our experimental values obtained for *Hm* MalDH in viscous solvents containing a high content of salt or organic solvent. The same procedure was applied with $s^\circ = 7$ S and $D^\circ = 5 \times 10^{-7}$ cm^2 s^{-1}, which approximate the values for the same particle in water. To obtain good starting guesses and avoid local minima in the nonlinear regres-

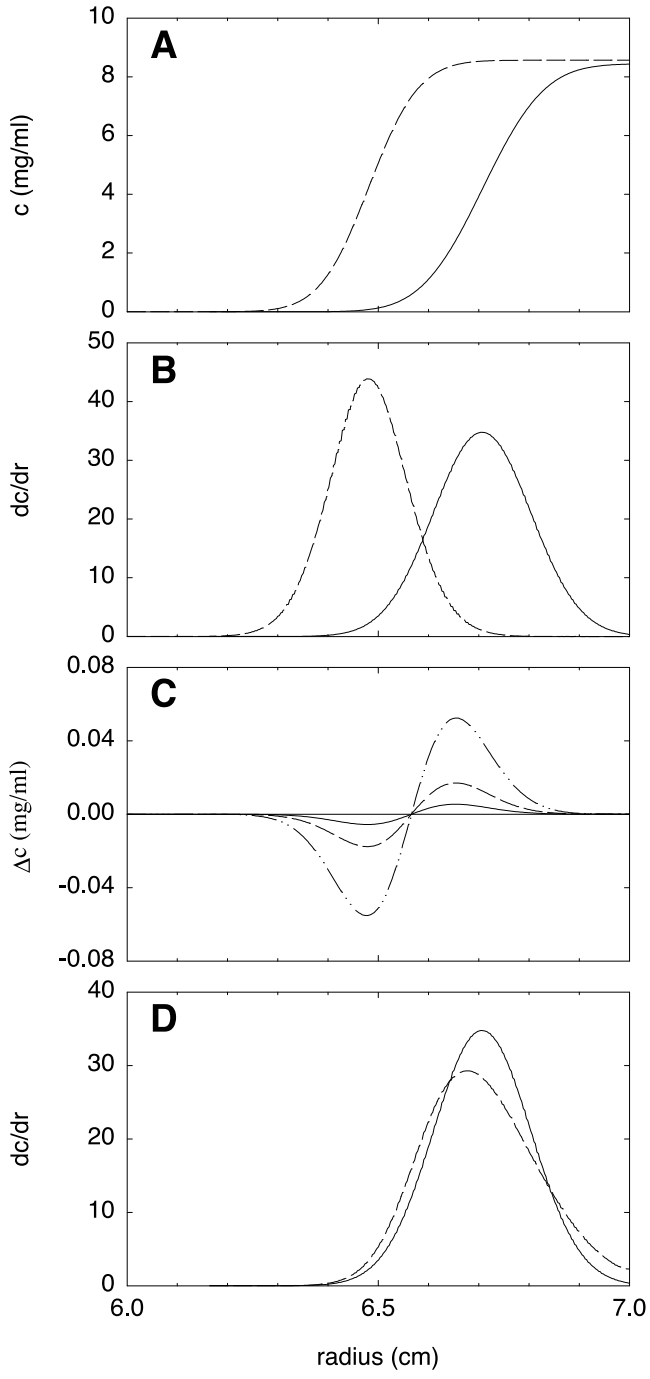

FIGURE 1 Effect of the concentration dependence of sedimentation and diffusion coefficients on sedimentation profiles. Shown are the theoretical concentration distributions of a solute with $s° = 2.5$ S, $D° = 2.5 \times 10^{-7}$ cm^2 s^{-1} and different non-ideality parameters k_s and k_D, calculated for an initially uniform loading concentration of 10 mg/ml, after 17,500 s of sedimentation at a rotor speed of 42,000 rpm. (*A* and *B*) Theoretical boundary profiles (*A*) and radial derivatives (*B*) are compared for ideal solutes (——) and for concentration-dependent sedimentation with $k_s = 10$ ml/g and $k_D = 0$ (— — —). (*C*) Calculated differences of ideal boundary profiles and those with concentration-dependent diffusion coefficient at $k_s = 0$ and $k_D = 1$ (——), 3 (— — —), and 10 (— · · —) ml/g. (*D*) Radial derivatives of the sedimentation boundary for $k_s = 0$ and $k_D = 0$ (——) and $k_D = 100$ ml/g (— — —).

sion, we choose a fitting procedure in three steps. First, the system is modeled as an ideal one, i.e., with the constraint $k_s = k_D = 0$. As a result, apparent values of s and D are obtained. These values are introduced as starting values for the second fit, in which only the concentration dependency of s is considered; i.e., $k_D = 0$, and log k_s is treated as an additional floating parameter, with a starting value of $k_s = 0.01$ ml/g. The third step starts with the values obtained after the second fit, and log k_D is also optimized together with $s°$, $D°$, and k_s, with an initial guess of $k_D = 0.01$ ml/g. This procedure was applied to the case of repulsive interactions (positive coefficients k_s and k_D) and to attractive interactions (negative coefficients). The numerical results of this procedure are given in Table 1. They are qualitatively similar for the two sets of generated data and detailed below for the closest to our experimental system. As can be expected, the first fitting step leads to the apparent s values that are close to the collective calculated s values of 1.78 S and 2.29 S, using Eq. 8, for repulsive and attractive cases, respectively. However, at this stage, the quality of the fit is poor (as judged from both the overall root mean square deviation (rmsd) and the systematic residuals), and the fitted values of the diffusion coefficient do not have a physical meaning. It should be noted that they are not the collective D values of Eq. 9. After the second step, in general, values for $s°$, D, and k_s are obtained that are close to the ones underlying the simulation. The rmsd of the fit is significantly improved, and residuals were nearly randomly distributed. However, we noted that $s°$ and k_s can be slightly correlated; an example of this is the underestimated $s°$ combined with an underestimated k_s shown in Table 1 for the repulsive case. However, this situation was improved after the third step, after which the parameter values converged to those underlying the simulation with a good accuracy. Correspondingly, the boundary profiles were well described, and for the repulsive case, a further significant drop in the rmsd was observed, indicating that the obtained parameter values are well defined.

These results demonstrate that already a single set of sedimentation profiles should contain sufficient information to obtain good estimates of $s°$, $D°$, k_s, and k_D. At first, this may seem surprising, as qualitatively, k_s and k_D modulate the shape of the sedimentation boundary in opposite ways. For example, in the case of repulsion, there is a strong sharpening of the boundary associated with the fact that s decreases with c and a slight broadening of the boundary related to the fact that D increases with c. However, it can be easily demonstrated that there are very significant quantitative differences. If we model the data generated with $k_s = k_D = 12.5$ ml/g with only a concentration dependency of the diffusion coefficient, we obtain a quality of fit similar to the impostor ideal model. Likewise, when we generated data with $k_s = 0$ and $k_D = 12.5$ ml/g, modeling with either the ideal model, or with $k_s \neq 0$ and $k_D = 0$, provides the same quality of fit (rmsd = 0.014 and the same systematic

TABLE 1 Modeling of simulated concentration distributions in non-ideal sedimentation

Input	Fitting steps	s (S)		D (10^{-7} cm^{2}s^{-1})		k_s (ml/g)		k_D (ml/g)		rmsd (fringes)	
		rep	attr	rep	attr	rep	attr	rep	attr	rep	attr
$s°$ = 2 S $D°$ = 1.5 × 10^{-7} cm^{2}s^{-1}, $\|k_s\| = \|k_D\|$ = 12.5 ml/g	Step 1: $k_s = k_D = 0$	1.79	2.26	0.98	2.68					0.037	0.049
	Step 2: $k_s \neq 0$, $k_D = 0$	1.85	2.02	1.61	1.49	4	−11.8			0.028	0.014
	Step 3: $k_s \neq 0$, $k_D \neq 0$	2.00	2.02	1.54	1.55	13.2	−11.9	11.5	−9	0.010	0.011
$s°$ = 7 S $D°$ = 5 × 10^{-7} cm^{2}s^{-1}, $\|k_s\| = \|k_D\|$ = 12.5 ml/g	Step 1: $k_s = k_D = 0$	6.3	7.9	3.0	9.5					0.068	0.078
	Step 2: $k_s \neq 0$, $k_D = 0$	7.1	7.2	5.6	5.7	14	−10			0.012	0.024
	Step 3: $k_s \neq 0$, $k_D \neq 0$	7.0	7.1	5.2	5.7	13	−10	10	−10	0.011	0.018

Concentration distributions were calculated for a rotor speed of 42,000 rpm, based on an initial concentration of 10 mg/ml, with k_s and k_D positive in the repulsive case (rep) and negative in the attractive one (attr). Normally distributed noise of 0.01 was added to the distributions. The fit was performed on 30 or 20 radial profiles taken in time intervals of 500 or 600 s after an initial sedimentation of 10,000 or 600 s, for s^o of 2 S and 7 S data, respectively.

distribution of residual), but when we allowed both k_s and k_D to float in modeling these data, the parameters converged to k_s = 0.3 ml/g and k_D = 10 ml/g, similar to the input parameters (rmsd = 0.010 and unsystematic residuals). Thus, when considering the evolution of the sedimentation boundary, k_s and k_D have distinctly different quantitative effects that can be distinguished by direct boundary modeling. The confidence in these parameters can be further improved by global modeling of experiments at different loading concentrations and rotor speeds, as will be shown in the following.

Sedimentation analysis of halophilic malate dehydrogenase in complex solvents

The modeling strategy outlined above was applied to the sedimentation profiles of concentrated halophilic malate dehydrogenase (*Hm* MalDH) at three different protein concentrations and in three different solvents at pH 8. Under the conditions used in these studies, *Hm* MalDH behaved as a stable tetramer, in agreement with previous sedimentation velocity experiments (Hecht and Jaenicke, 1989). Although some dissociation was observed in sedimentation equilibrium at pH 7 (Bonneté et al., 1993), we have seen no evidence of this at pH 8, which is consistent with a clear transition in the protein stability between pH 7 and pH 8 observed earlier (Madern and Zaccai, 1997). Therefore, we can apply the single-component analysis developed above to tetrameric *Hm* MalDH as an experimental test.

In a first approach, 9–10 scans taken in intervals of 40 or 50 min were analyzed. As an example, Fig. 2 shows the experimental and best-fit distributions, and the differences between them (residuals), for a protein loading concentration of 12 mg/ml in 4 M NaCl. Even when neglecting non-ideality (Fig. 2, *A* and *B*), the experimental curves are not too badly described by the model. Considering non-ideality in the second and third fitting step improves, however, the quality of the fit as can be judged from the decreased absolute values and the more random distribution of the residuals (Fig. 2, *C* and *D*). Table 2 gives the detailed

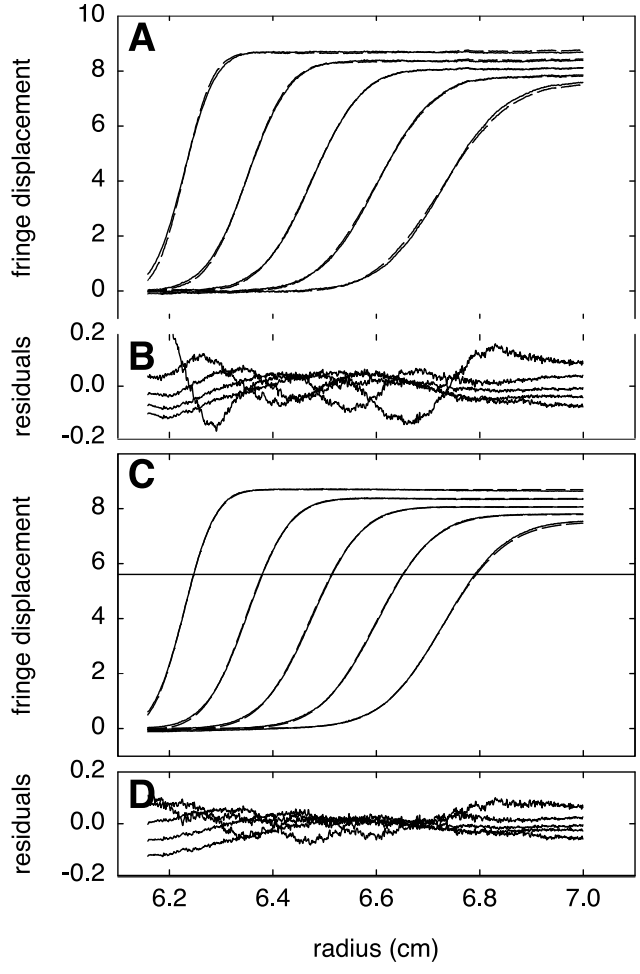

FIGURE 2 Modeling of the sedimentation profiles of *Hm* MalDH at 12.3 mg/ml in 4 M NaCl. (*A* and *C*) Experimental fringe displacement distributions (——) and best-fit distributions (— — —) from sedimentation velocity performed at 42,000 rpm at 20°C in 3-mm cells; (*B* and *D*) Residuals. Ideal sedimentation modeling ($k_s = k_D = 0$) on *A* and *B* resulted in an s value of 2.06 S and an apparent D-value of 2.0 × 10^{-7} cm^2 s^{-1}, with a rmsd of 0.059 fringe (see text). Non-ideal modeling ($k_s \neq 0$,) on *C* and *D*, resulted in $s°$ = 2.35S, $D°$ = 3.2 × 10^{-7} cm^2 s^{-1}, k_s = 12 ml g^{-1}, and k_D = 1 ml g^{-1} with a rmsd of 0.039 fringe. For clarity, only every second profile that was used in the analysis is shown.

TABLE 2 Modeling of sedimentation velocity profiles of *Hm* MalDH

	Ideal fit				Non-ideal fit with $k_s \neq 0$				Non-ideal fit with $k_s \neq 0$, $k_D \neq 0$				
	c (mg/ml)	s (S)	D_{app} (10^{-7} cm^{2}s^{-1})	rmsd	$s°$ (S)	D (10^{-7} cm^{2}s^{-1})	k_s (ml/g)	rmsd	$s°$ (S)	$D°$ (10^{-7} cm^{2}s^{-1})	k_s (ml/g)	k_D (ml/g)	rmsd
4 M NaCl	12.3	2.06	2.0	0.059	2.37	3.2	13	0.038	2.35	3.2	12	1	0.039
	4.43	2.26	2.1	0.043	2.34	3.1	9	0.033	2.34	3.1	9	2.5	0.033
	2.21	2.36	3.1	0.013	2.40	3.4	11	0.014	2.39	3.2	8	2.5	0.014
Mean					2.37 ± 0.02	3.2 ± 0.1	11 ± 1		2.36 ± 0.01	3.1 ± 0.1	10 ± 2	2 ± 1	
Mean (10 sequential profiles)					*2.35 ± 0.02*	*2.9 ± 0.1*	*8 ± 1.5*		*2.36 ± 0.01*	*2.9 ± 0.1*	*8 ± 2*	*2 ± 1*	
Global modeling									2.42 ± 0.01	3.4 ± 0.1	14 ± 1	0 ± 1	
Global modeling of duplicate experiment									2.43	3.0	12	1	
Global modeling, 12-mm cells									2.41	3.2	9	0	
Global modeling, 12-mm cells, 60,000 rpm									2.41	2.9	11	1	
Global modeling, 12-mm cells, 60,000 rpm and 40,000 rpm									2.42	3.1	11	0	*0.074*
5% MPD + 2 M NaCl	7.29	3.62	2.4	0.034	3.81	3.2	8	0.032	3.81	3.2	8	8	0.032
	3.51	3.72	2.9	0.026	3.76	3.2	4	0.026	3.76	3.2	4	8	0.026
	1.46	3.75	3.1	0.010	3.77	3.2	6	0.010	3.77	3.1	6	8	0.010
Mean					3.78 ± 0.02	3.2 ± 0.1	6 ± 1		3.78 ± 0.03	3.2 ± 0.1	6 ± 2	8 ± 1	
Mean (10 sequential profiles)					*3.8 ± 0.02*	*3.0 ± 0.1*	*7 ± 1*		*3.81 ± 0.03*	*3.0 ± 0.1*	*7 ± 2*	*5 ± 4*	
Global modeling									3.83 ± 0.01	3.2 ± 0.1	9 ± 1	0 ± 5	
30% MPD + 1.5 M NaCl	6.87	1.96	2.3	0.092	1.78	1.3	−15	0.087	1.78	1.3	−15	−6	0.087
	3.39	1.84	1.3	0.062	1.80	1.2	−7	0.062	1.79	1.6	−9	−7	0.062
	1.46	1.82	1.4	0.030	1.79	1.4	−10	0.030	1.79	1.4	−9	−7	0.030
Mean					1.79 ± 0.01	1.3 ± 0.1	−11 ± 2		1.78 ± 0.01	1.4 ± 0.1	−11 ± 2	−7 ± 1	
Mean (10 sequential profiles)					*1.68 ± 0.04*	*0.8 ± 0.2*	*−22 ± 6*		*1.70 ± 0.03*	*0.9 ± 0.1*	*−17 ± 3*	*−2 ± 1*	
Global modeling									*1.72 ± 0.01*	*1.1 ± 0.1*	*−18 ± 1*	*−3 ± 2*	

Experimental fringe displacement profiles of *Hm* MalDH sedimenting in 3 mm cells at 42,000 rpm were analyzed, unless noted otherwise. Time intervals of the scans used for analysis was ~45 min. (regular type) or 4 to 5 min. (italics), respectively. Global modeling was performed using only every 5th or 10th scans for each cell.

outputs obtained after each of the three fitting steps, for three protein concentrations and three different solvents. In 4 M NaCl, fitting with the ideal model (step 1) gives sedimentation coefficients that decrease with increasing protein concentration, a behavior that is commonly observed and typical of overall repulsive interactions. Consistent with the simulation studies described above, the second step reduces the rmsd significantly, except for the more diluted sample. It should be noted that the sedimentation coefficients $s°$ corresponding to infinite dilution, the diffusion constants D, and the k_s values obtained after this second step are similar for each dilution. Allowing for a concentration dependency in D in the third step also provides similar values for k_D for all experiments. However, this last step does not improve the quality of the fit significantly. This indicates that the k_D values could be poorly determined.

Using this approach, a difficulty was encountered in the analysis of complex solvents near the phase separation, such as salt-MPD mixtures at high solute concentrations (Richard et al., 1995; Pittz and Timasheff, 1978). When the solvent composition is close to the coexistence curve between one-liquid and two-liquid phases in the phase diagram, we observed strong distortions in the interference optical signals, in particular, in the proximity of the meniscus, which are probably related to solvent redistribution at the interfaces. These distortions were reproducibly observed in the present study for 1.5 M NaCl, 30% MPD (and were also observed for mixtures of ammonium sulfate and MPD for compositions close to phase separation; data not shown). As a consequence, modeling the complete sedimentation process (Fig. 3, *A* and *B*) does not lead to very good fits, despite the algebraic calculation of the time-invariant and radial-invariant systematic noise components of the interference signal. As an alternative approach, we analyzed the data with more closely spaced scans (4–5-min intervals) after the boundary was localized in the middle of the cell, thereby avoiding the perturbed region near the meniscus. As can be seen in Fig. 3, *C* and *D*, these boundaries were significantly better described by the model. The resulting best-fit parameters with this approach are given in Table 2 (data in italics). For each of the three solvents, similar values for $s°$, $D°$, and k_s were obtained for the three protein concentrations. For 1.5 M NaCl, 30% MPD, the numerical values differ slightly from the analysis of scans with larger time intervals but remain in the same order of magnitude. For the experiments in 4 M NaCl and in 2 M NaCl, 15% MPD, far from phase separation, the best-fit values are very similar to those from larger time intervals. This indicates that this approach can also be successful, even though the improvement of the quality of the fit from step to step is much smaller.

It is clear from inspection of Table 2 that for all of the three investigated solvents, self-consistent results are obtained, with very similar values for the fitted parameters independent of the selection of the boundary profiles and

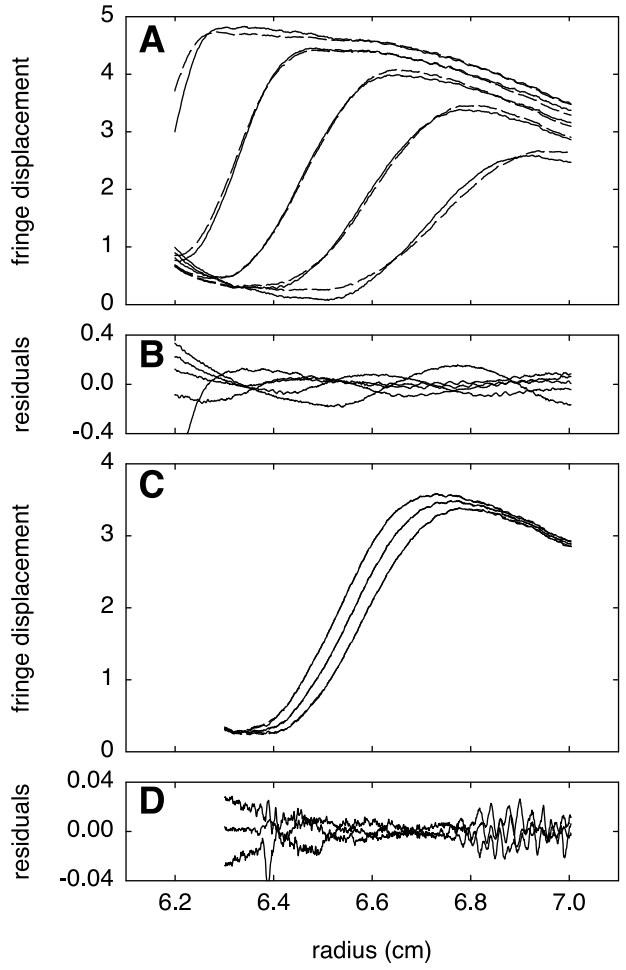

FIGURE 3 Non-ideal modeling of the sedimentation profiles of *Hm* MalDH at 6.9 mg/ml in 1.5 M NaCl, 30% MPD. (*A* and *C*) Experimental fringe displacement distributions (——) and best-fit distributions of the non-ideal model with $k_s \neq 0$, $k_D \neq 0$ (— — —) from sedimentation velocity performed at 42,000 rpm at 20°C in 3-mm cells; (*B* and *D*) Residuals. On *A* and *B*, the analysis of nine profiles with large time intervals (every second profile shown) that resulted in $s° = 1.78$ S, $D° = 1.3 \times 10^{-7}$ cm^2 s^{-1}, $k_s = -15$ ml g^{-1}, and $k_D = -6$ ml g^{-1} with a rmsd of 0.087 fringe. On *C* and *D*, the analysis of 10 closely spaced scans (showing scans 1, 5, and 9) that resulted in $s° = 1.65$ S, $D° = 0.7 \times 10^{-7}$ cm^2 s^{-1}, $k_s = -23$ ml.g^{-1}, and $k_D = -2$ ml g^{-1} with a rmsd of 0.006 fringe.

loading concentrations. This suggests that the model used for the description of the boundary profile is essentially correct. A global fitting procedure was thus applied to determine more precisely the four global parameters ($s°$, $D°$, k_s, and k_D) characterizing the transport of the non-ideal material.

The same general procedure can be followed as described above. From local ideal modeling of the profiles corresponding to each protein concentration, we can estimate quickly if the inter-particle effects are large, and repulsive or attractive. Further, we can define the starting conditions for non-ideal modeling from the more diluted sample. Then,

TABLE 3 Thermodynamic and hydrodynamic parameters of *Hm* MalDH from modeling of the non-ideal sedimentation compared with other methods

	$s°$ (S)	$D°$ (10^7 cm^{2}s^{-1})	$M(\partial\rho/\partial c)_{T,\mu_S}$ (kg/mol)	$M(\partial\rho/\partial c)_{T,\mu_S}$ in NaCl (kg/mol)	$\rho°$ (g/ml)	k_s (ml/g)	k_D (ml/g)	$2A_2M$ ($k_s + k_D$) (ml/g)	$2A_2M$ (SANS) (ml/g)
4 M NaCl, non-ideal boundary model from	2.41	3.1	21	21	1.153	12	0	13	9
apparent $s(c)$ and $D(c)$	2.41	2.6; 3.1	23			14	3	17	
5% MPD, 2 M NaCl, non-ideal boundary	3.83	3.2	29	32	1.079	9	0	9	7
model from apparent $s(c)$ and $D(c)$	3.8					8			
30% MPD, 1.5 M NaCl, non-ideal boundary	1.72	1.1	37	39	1.047	−18	−3	−21	−26
model from apparent $s(c)$ and $D(c)$	1.73	1.5	28			−13	−2	−15	

Values are given for the direct global boundary modeling (reproduced from Table 2), from the extrapolation of the concentration dependence of s values from a series of traditional sedimentation velocity analyses, and from the concentration dependence of the diffusion coefficients by dynamic light scattering (Fig. 4; or from Pittz and Timasheff, 1978). The two columns for the buoyant molar masses $M(\partial\rho/\partial c)_{T,\mu_S}$ are from combining $s°$ and $D°$ and from combining density increments $(\partial\rho/\partial c)_{T,\mu_S}$ measured by Bonneté et al. (1993) in NaCl solutions with the molar mass of a stable *Hm* MalDH tetramer, respectively (see text). In the two last columns, the second virial coefficient terms $2A_2M$ from boundary modeling are compared with those obtained from SANS by Costenaro et al. (2001), in 4 M NaCl, 5% MPD, 1.5 M NaCl, and 30% MPD, 1.5 M NaCl, respectively.

the quality of the modeling is estimated globally, from the value of the global reduced χ^2. The precision of the global parameters for each set of experimental data was estimated by varying the initial conditions of the fit. The values obtained for $s°$, $D°$, and k_s are similar to those derived from individual data sets. Values for k_D are in general smaller and appear as nearly indistinguishable from instrumental noise, with absolute value of k_D equal or above 3 ml/g.

We also studied the reproducibility of the global modeling results for different experimental conditions. The results obtained with data from three loading concentrations of *Hm* MalDH in 4 M NaCl acquired using either 3- or 12-mm-thick cells, at 42,000 or 60,000 rpm are given in Table 2. Similarly, a global modeling of data from different rotor speeds and loading concentrations was performed. Although these measurements were performed on different *Hm* MalDH preparations, the parameters are very consistent. $D°$ is obtained with a precision of 10%. However, the residuals are not always randomly distributed, as can be seen on Figs. 2 and 3, which could be attributed, in part, to the remaining systematic noise from the data acquisition. On the other hand, it should be considered that the additional constraints imposed by global analysis necessarily leads to an increase in the rms error, and that rms error in the global fit of 0.07 still represents a fit with a relative error of only 0.4%, due to the high loading concentrations. To study the possibility of systematic errors from modeling, we compared the best-fit results with those obtained from other techniques. This comparison is summarized in Table 3.

Comparison of the parameters for the ideal particle the non-ideality coefficients k_s and k_D with those from other experimental approaches

An alternative, more traditional analysis of the sedimentation coefficients is an initial interpretation of the sedimentation data with a model for an ideal apparent particle, followed by the regression of the determined sedimentation coefficients $s(c)$ as a function of concentration according to Eq. 8. Although this approach requires several experiments at different concentrations, it also can estimate the extrapolated sedimentation coefficient at infinite dilution, $s°$, and the non-ideality coefficient k_s. This approach is shown in Fig. 4 *A*. It results in $s°$ values that are very similar to those

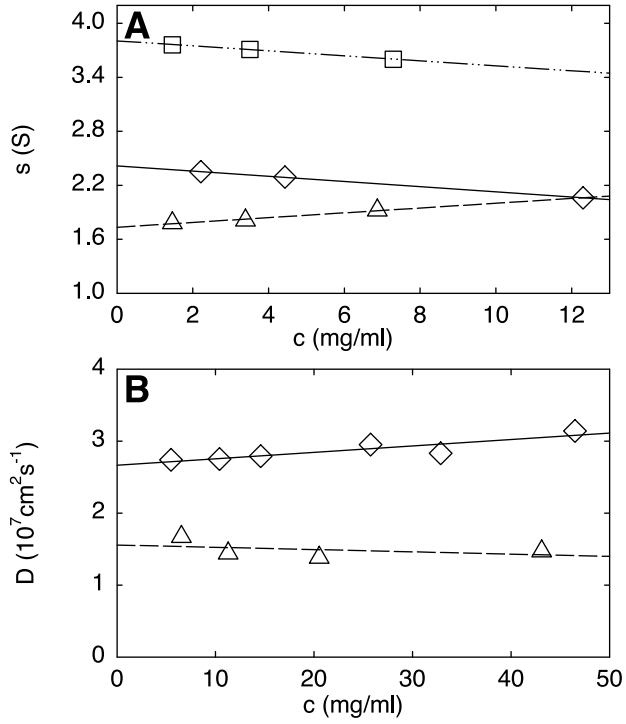

FIGURE 4 Linear regression of the mean sedimentation and diffusion coefficients measured as a function of *Hm* MalDH concentration. (*A*) Sedimentation coefficients s evaluated from modeling of sedimentation profiles as a single ideal component; (*B*) Diffusion coefficients D_{20} from dynamic light scattering. Solvents were 4 M NaCl (◇), 5% MPD + 2 M NaCl (□), and 30% MPD + 1.5 M NaCl △.

from non-ideal boundary modeling and also in k_s values of similar magnitude (see Table 3).

An analogous procedure can be applied to the concentration dependence of the collective diffusion coefficient measured by the exponential decay of the autocorrelation function from DLS (see Experimental Procedures and Theoretical Background above). For weakly interacting particles, the collective diffusion coefficient in DLS is the same as measured by sedimentation experiments if the characteristic distance $2\pi/q$ is much larger than the mean inter-particle distance and if the characteristic decay times of the autocorrelation function τ are much larger than the time scale of the macromolecular interactions τ_I (Pusey and Tough, 1985). These conditions are fulfilled in our experiments. $2\pi/q \approx 3000$ Å, which is large compared with the inter-macromolecular distances (~600 Å and 130 Å for protein concentration of 1 and 100 mg/ml, respectively). For the protein in 4 M NaCl, for example, we measured a characteristic decay time τ of 70 μs, whereas the maximal value for τ_I (estimated as the time needed for a protein to freely diffuse the average inter-macromolecular distance, $L^2/D°$) for a protein concentration of 1 mg/ml in the same solvent would be ~20 μs and much smaller in more concentrated solutions.

Light-scattering experiments were performed for *Hm* MalDH concentrations in the range 5–50 mg/ml in two solvents. The auto-correlation functions were described well by a single-exponential decay in 4 M NaCl and a double-exponential decay in 1.5 M NaCl, 30% MPD (the slower decay with $D \approx 0.4 \times 10^{-7}$ cm^2 s^{-1} is attributed to the solvent fluctuations). Typical baseline values were 1.01–1.02, which is reasonable compared with the theoretical expectation value of unity. Values of $D°$ and k_D were obtained assuming a linear concentration dependency of D according to Eq. 9 (Fig. 4 *B*) and are listed in Table 3. Unfortunately, we found that D values in the mixed NaCl-MPD solvent are not very precise, and large errors are associated with the estimated k_D in the two solvents. However, the k_D values determined by DLS are in qualitative agreement with those determined from non-ideal modeling of the sedimentation boundary profiles, despite the large relative error in both experiments (see above). When comparing the $D°$ values from non-ideal boundary modeling, from DLS and from literature values (Pundak and Eisenberg, 1981), we found similar, although not identical, values. It should be noted, however, that the two types of experiments were not performed on the same samples and that slight variations in the solvent composition are possible that may affect diffusion coefficients.

A further possibility for independent validation of the $s°$ and $D°$ values from non-ideal modeling of the sedimentation boundary represents the comparison of buoyant molar mass values $M(\partial\rho/\partial c)_{T,\mu_S}$, which is determined by the ratio of $s°$ and $D°$ (Eq. 7). In the present study, the most important aspect in confirming the buoyant molar masses is the evaluation of the $D°$ estimate, as this parameter is derived solely from the shape of the sedimentation boundary. In the case of a complex solvent, the density increment $(\partial\rho/\partial c)_{T,\mu_S}$ is determined not only by the solvent density but also by the interactions between the macromolecule and the solvent components (Eisenberg, 1976; Ebel, 1995). We calculated $M(\partial\rho/\partial c)_{T,\mu_S}$ on the basis of tetrameric *Hm* MalDH of molar mass 130.5 kDa from the experimental values of $(\partial\rho/\partial c)_{T,\mu_S}$ measured by Bonneté et al. (1993). Because the $(\partial\rho/\partial c)_{T,\mu_S}$ values were obtained from density measurements on the protein in NaCl solutions, we interpolated the data to solvents of a density equal to the density of our complex solvents used for the sedimentation experiments. This results in buoyant molar mass values that are in good agreement for all three solvents (Table 3), which suggests the reliability of our $D°$ estimate from non-ideal modeling of the boundary shape. Interestingly, for the solvent close to phase separation (30% MPD and 1.5 M NaCl), the determination of $D°$ from the non-ideal sedimentation boundary appears to be superior to the estimate from DLS. However, one important consideration in this respect could be that in sedimentation experiments, both $s°$ and $D°$ are determined strictly in the same buffer, a feature that could be important, in particular, in the context of studies in complex solvents.

By comparing the $(\partial\rho/\partial c)_{T,\mu_S}$ values in NaCl and mixed NaCl-MPD solvents, we assume that the density of the solvated protein, i.e., of its solvation shell, is not much affected by the presence of MPD. This hypothesis is reasonable, even if MDP is excluded from the proximity of the protein, as described (in the absence of salt) for bovine pancreatic ribonuclease A from differential refractometry (Pittz and Timasheff, 1978). Changes in the water and MPD concentrations in the proximity of the protein are not expected to affect significantly the values of the buoyant molar mass of the protein, because the partial specific volumes of water and MPD are very similar. For this reason, and because the buoyant molar masses are estimated here only with a precision of ~10–15%, our measurements will not be discussed in terms of protein-solvent interactions.

From the comparisons above, we can conclude that the non-ideal boundary modeling of sedimentation profiles at high protein concentration in the presence of inter-particle interactions allows a good estimate of the properties of the ideal particle, in terms of both its sedimentation and diffusion coefficient.

Comparison of the second virial coefficients with SANS and with theory

The second virial coefficient can be calculated from k_s and k_D using Eq. 11. The resulting values, expressed as $2A_2M$, are listed in Table 3. They can be compared with the values measured previously from small-angle neutron scattering (SANS) (Ebel et al., 1999b; Costenaro et al., 2001). (The values in the solvent for 5% MPD was reported by SANS

for 1.5 M NaCl, which we expect to be very close to the slightly higher NaCl concentration of 2 M used in the present study.) For each of the solvent conditions, the second virial coefficient values obtained from modeling of the sedimentation boundary profiles and from SANS experiments are of the same order of magnitude and of reasonably good agreement, which seems sufficient for our goal of screening different solvent conditions for approximate values and changes in the sign of the virial coefficient.

In the present study, the values of k_s, k_D, and $2A_2M$ have the same sign and k_D was smaller than k_s. This suggests that a qualitative investigation of the whole particle interactions may be made already from the value of k_s alone. Because the sedimentation profiles are highly disturbed by the concentration dependence of the sedimentation coefficient, the determination of k_s is very robust, in non-ideal boundary modeling or even simply from the evaluation of the apparent s value at different protein concentrations. This simplification could be justified theoretically on the basis that k_D should be small compared with k_s for non-interacting spheres, because the collective diffusion coefficient is determined by partial cancellation of the thermodynamic factor $(\partial\Pi/\partial C)_{T,\mu_s}$ and the hydrodynamic ones (friction coefficient) (see Eqs. 6 and 11). An exception would be the case, for example, of particles interacting through long-range direct interactions, such as charged macromolecules in pure water (Pusey and Tough, 1985; Retailleau et al., 1997). Also, k_D/k_s ratios between 0.3 and 0.6 were reported from experimental studies with turnip-yellow-mosaic virus in non-dissociating solvents (Harding and Johnson, 1985b), and ratios of 1 or larger were estimated for γ-crystallins in attractive or repulsive regimes of inter-particle interactions (Bonneté et al., 1997).

The small absolute values for k_D found in the range 0–3 ml/g from global direct modeling of the sedimentation profiles were confirmed by DLS, in our attractive and repulsive conditions. Clearly, global fitting procedure avoided an overestimation of k_D. As a consequence, a very good correlation is found in Table 3 for k_S, k_D, and $2A_2M_2$ obtained through different techniques. It should be noted that, in 4 M NaCl, the values $k_D = 0$–3 ml/g and $k_s \approx 2A_2M_2 \approx 12$–13 ml/g are compatible with the theoretical ratios k_D/k_S and $k_D/2A_2M_2$ predicted for non-interacting hard spheres, which are 0.25 and 0.2, respectively (Pusey and Tough, 1985). In this solvent, it is reasonable to consider this protein as a non-interacting hard sphere, because globular *Hm* MalDH is very soluble (above 200 mg/ml) and electrostatic interactions can be neglected in 4 M NaCl. Furthermore, for non-interacting hard spheres, the virial term $2A_2M$ is related to v_s, the swollen specific volume, or R, the corresponding radius according to $2A_2M = 8v_s = (N_A/M)32/3\pi R^3$ (Tanford, 1961). Using our $2A_2M$ values of 13 ml/g or 17 ml/g in 4 M NaCl, we can calculate radii of 44 or 48 Å, which are close or slightly larger than the radius of 40 Å estimated from the largest dimension of the globular *Hm* MalDH in the high-resolution structure (Dym et al., 1995). At higher MPD concentration, finally, we found the negative value of $2A_2M$ of ~ -20 ml/g ($A_2 = -8 \times 10^{-5}$ ml mol g^{-2}) in 30% MPD, 1.5 M NaCl, which is indicative of moderately attractive intermolecular interactions described to be favorable to protein crystallization (George and Wilson, 1994). This is in agreement with the fact that the composition of this solvent is close to that in which our protein crystallizes nicely (Richard et al., 1995; Costenaro et al., 2001).

CONCLUSION

In the present study, we have shown that sedimentation velocity combined with direct boundary modeling using the Lamm equation for non-ideal sedimentation can be used to investigate weak interactions. Although the concept of positive and negative virial coefficients for expressing global attraction and repulsion is not appreciated by many traditional biochemists, this approach can describe both attractive and repulsive interactions, with positive and negative values for k_s, k_D, and A_2, respectively. Many authors describe attractive interactions as specific contacts between well-defined macromolecular species and, accordingly, relate non-ideality only to intermolecular repulsive contributions, i.e., excluded volume and electrostatic repulsion (Behlke and Ristau, 1999). With these assumptions, the second virial coefficient is always positive and can be calculated considering the shape, hydration, and charge of the macromolecules, as was done, for example, considering modeled ellipsoids (Harding et al., 1999). A low or negative value, corresponding to attractive conditions, is then interpreted in terms of macromolecular association related to an equilibrium between different oligomeric forms of the protein. However, in the case of weak attractive interactions, the proposed association process is generally very complex, because it is characterized by a large number of polymeric species, and corresponding association constants can hardly be discriminated (Behlke and Knespel, 1996; Winzor and Wills, 1994; Wills et al., 1980). It is then a fruitful approach to describe weak interactions in undersaturated protein solutions in terms of simple potentials between modeled homogeneous species. For example, x-ray scattering curves for lysozyme in various conditions have been modeled considering three simple spherical potentials, and reasonable parameters for the protein diameter and charge and attractive potential depth and range has allowed the description of macromolecular phase diagrams, pH effects, and nonspecific salt effects (Malfois et al., 1996; Ducruix et al., 1996; Tardieu et al., 1999). In these descriptions, specific solute-solvent interactions have not been modeled. However, more complex potentials, in which, for example, the solvent is not a continuum, or with a more precise description of the protein, are being studied for improving the description of inter-particle interactions and for investigat-

ing the specific effects of salts on crystallogenesis (Georgalis and Saenger, 1999; Piazza, 1999; Belloni, 1991).

The understanding of the effects of solvent composition on global inter-particle interactions is a first step for the understanding of protein crystallization processes in complex solvents. We have shown here that sedimentation velocity can be a good technique for this purpose. The protocol applied uses less than two recoverable milligrams of protein for each solvent condition. Complex solvents can be investigated, containing high concentrations of salt and organic compounds close to phase separation. By global direct boundary modeling of interference optical ultracentrifuge data combined with systematic noise decomposition, one can take advantage of the high sensitivity and the high dynamic range of the detection system. Because $s°$ and $D°$ values are obtained with a relatively good precision, this procedure should be generally useful for the characterization of the molar masses and hydrodynamic properties of asymmetric or charged solutes displaying large non-ideality. As discussed above, both attractive and repulsive interactions can be described, with positive and negative values for k_s, k_D, and A_2, respectively. Importantly, the second virial coefficient can be determined with an accuracy that appears sufficient to screen different solvent conditions for changes of globally repulsive to globally attractive interactions. In the present study, we observed such a change in the sign of the weak interactions for halophilic malate dehydrogenase in mixed NaCl-MPD, which is clearly related to the capacity of the protein either to remain soluble or to crystallize in solution.

REFERENCES

Behlke, J., and A. Knespel. 1996. Observation of precrystallisation aggregation in protein solutions during centrifugation. *J. Crystal Growth.* 158:388–391.

Behlke, J., and O. Ristau. 1997. Molecular mass determination by sedimentation velocity experiments and direct fitting of the concentration profiles. *Biophys. J.* 72:428–34.

Behlke, J., and O. Ristau. 1999. Analysis of the thermodynamic nonideality of proteins by sedimentation equilibrium experiments. *Biophys. Chem.* 76:13–23.

Belloni, L. 1991. Interacting monodisperse and polydisperse spheres. *In* Neutron, X-Ray and Light Scattering: Introduction to an Investigative Tool for Colloidal and Polymeric Systems. Elsevier Science Publishers, New York. 135–155.

Bonneté, F., C. Ebel, H. Eisenberg, and G. Zaccai. 1993. Biophysical study of halophilic malate dehydrogenase in solution: revised subunit structure and solvent interactions in native and recombinant enzyme. *J. Chem. Soc. Faraday Trans.* 89:2659–2666.

Bonneté, F., S. Finet, and A. Tardieu. 1999. Second virial coefficient: variations with lysozyme crystallization conditions. *J. Crystal Growth.* 196:403–414.

Bonneté, F., M. Malfois, S. Finet, A. Tardieu, S. Lafont, and S. Veesler. 1997. Different tools to study interaction potentials in γ-crystallin solutions: relevance to crystal growth. *Acta Cryst.* D53:438–447.

Cendrin, F., J. Chroboczek, G. Zaccai, H. Eisenberg, and M. Mevarech. 1993. Cloning, sequencing, and expression in *Escherichia coli* of the gene coding for malate dehydrogenase of the extremely halophilic archaebacterium *Haloarcula marismortui*. *Biochemistry.* 32: 4308–4313.

Claverie, J. M. 1976. Sedimentation of generalized systems of interacting particles. III. Concentration-dependent sedimentation and extension to other transport methods. *Biopolymers.* 15:843–57.

Costenaro, L., G. Zaccai, and C. Ebel. 2001. Understanding protein crystallisation by dilution: the ternary NaCl-MPD-H_2O system. *J. Crystal Growth.* 232:102–113.

Demeler, B., and H. Saber. 1998. Determination of molecular parameters by fitting sedimentation data to finite-element solutions of the Lamm equation. *Biophys. J.* 74:444–54.

Dishon, M., G. H. Weiss, and D. A. Yphantis. 1967. Numerical solutions of the Lamm equation. III. Velocity centrifugation. *Biopolymers.* 5:697–713.

Ducruix, A., J. P. Guilloteau, M. Ries-Kautt, and A. Tardieu. 1996. Protein interactions as seen by solution x-ray scattering prior to crystallogenesis. *J. Crystal Growth.* 168:28–39.

Dym, O., M. Mevarech, and J. L. Sussman. 1995. Structural features that stabilize halophilic malate dehydrogenase from an *archaebacterium. Science.* 267:1344–1346.

Ebel, C. 1995. Characterisation of the solution structure of halophilic proteins. Analytical centrifugation among complementary techniques (light, neutron and x-ray scattering, density measurements). *Prog. Colloid Polymer Sci.* 99:17–23.

Ebel, C., P. Faou, B. Franzetti, B. Kernel, D. Madern, M. Pascu, C. Pfister, S. Richard, and G. Zaccai. 1998. Molecular interactions in extreme halophiles: the solvation-stabilization hypothesis for halophilic proteins. *In* Microbiology and Biogeochemistry of Hypersaline Environments. CRC Press, Boca Raton, FL. 227–237.

Ebel, C., P. Faou, B. Kernel, and G. Zaccai. 1999a. Relative role of anions and cations in the stabilization of halophilic malate dehydrogenase. *Biochemistry.* 38:9039–9047.

Ebel, C., P. Faou, and G. Zaccai. 1999b. Protein-solvent and weak protein-protein interactions in halophilic malate dehydrogenase. *J. Crystal Growth.* 196:395–402.

Eisenberg, H. 1976. Biological macromolecules and polyelectrolytes in solution. Clarendon Press, Oxford.

Eisenberg, H. 1981. Forward scattering of light, x-rays and neutrons. *Q. Rev. Biophys.* 14:141–172.

Fujita, H. 1975. Foundations of Ultracentrifugal Analysis. J. Wiley and Sons, New York.

Georgalis, Y., and W. Saenger. 1999. Light scattering studies on supersaturated protein solutions. *Sci. Prog.* 82:271–294.

George, A., Y. Chiang, B. Guo, A. Arabshahi, Z. Cai, and W. W. Wilson. 1997. Second virial coefficient as predictor in protein crystal growth. *Methods Enzymol.* 276:100–110.

George, A., and W. W. Wilson. 1994. Predicting protein crystallization from a dilute solution property. *Acta Cryst.* D50:361–365.

Guo, B., S. Kao, H. McDonald, A. Asanov, L. L. Combs, and W. W. Wilson. 1999. Correlation of second virial coefficients and solubilities useful in protein crystal growth. *J. Crystal Growth.* 196:424–433.

Harding, S. E., J. C. Horton, S. Jones, J. M. Thornton, and D. J. Winzor. 1999. COVOL: an interactive program for evaluating second virial coefficients from the triaxial shape or dimensions of rigid macromolecules. *Biophys. J.* 76:2432–2438.

Harding, S. E., and P. Johnson. 1985a. The concentration-dependence of macromolecular parameters. *Biochem. J.* 231:543–7.

Harding, S. E., and P. Johnson. 1985b. Physicochemical studies on turnip-yellow-mosaic virus: homogeneity, relative molecular masses, hydrodynamic radii and concentration-dependence of parameters in non-dissociating solvents. *Biochem J.* 231:549–555.

Hecht, K., and R. Jaenicke. 1989. Malate dehydrogenase from the extreme halophilic archaebacterium *Halobacterium marismortui*: reconstitution of the enzyme after denaturation and dissociation in various denaturants. *Biochemistry.* 28:4979–4985.

Kernel, B., G. Zaccai, and C. Ebel. 1999. Determination of partial molal volumes, and salt and water binding of highly charged biological mac-

romolecules (tRNA, halophilic protein) in multimolar salt solutions. *Prog. Colloid Polymer Sci.* 113:168–175.

Lamm, O. 1929. Die Differentialgleichung der Ultrazentrifugierung. *Ark. Mat. Astr. Fys.* 21B:1–4.

Madern, D., and G. Zaccai. 1997. Stabilisation of halophilic malate dehydrogenase from *Haloarcula marismortui* by divalent cations: effects of temperature, water isotope, cofactor and pH. *Eur. J. Biochem.* 249: 607–611.

Malfois, M., F. Bonneté, L. Belloni, and A. Tardieu. 1996. A model of attractive interactions to account for fluid-fluid phase separation of protein solutions. *J. Chem. Phys.* 105:3290–3300.

MacMillan, W. G., and J. E. Mayer. 1945. The statistical thermodynamics of multicomponent systems. *J. Chem. Phys.* 13:276–305.

Piazza, R. 1999. Interactions in protein solutions near crystallisation: a colloid physics approach. *J. Crystal Growth.* 196:415–423.

Pittz, E. P., and S. N. Timasheff. 1978. Interaction of ribonuclease A with aqueous 2-methyl-2,4-pentanediol at pH 5.8. *Biochemistry.* 17:615–623.

Pundak, S., and H. Eisenberg. 1981. Structure and activity of malate dehydrogenase from the extreme halophilic bacteria of the Dead Sea. I. Conformation and interaction with water and salt between 5 M and 1 M NaCl concentration. *Eur. J. Biochem.* 118:463–470.

Pusey, P. N., and J. A. Tough. 1985. Particle interactions. *In* Dynamic Light Scattering: Applications of Photon Correlation Spectroscopy. Plenum Press, New York. 85–179.

Retailleau, P., M. Ries-Kautt, and A. Ducruix. 1997. No salting-in of lysozyme chloride observed at low ionic strength over a large range of pH. *Biophys. J.* 73:2156–2163.

Richard, S., F. Bonneté, O. Dym, and G. Zaccai. 1995. Protocol 21: the MPD-NaCl-H_2O system for the crystallization of halophilic proteins. *In* Archaea: A Laboratory Manual. Cold Spring Harbor Laboratory Press, New York. 149–153.

Richard, S. B., D. Madern, E. Garcin, and G. Zaccai. 2000. Halophilic adaptation: novel solvent protein interactions observed in the 2.9 and 2.6 Å resolution structures of the wild type and a mutant of malate dehydrogenase from *Haloarcula marismortui. Biochemistry.* 39:992–1000.

Rowe, A. J. 1992. The concentration dependence of sedimentation. *In* Analytical Ultracentrifugation in Biochemistry and Polymer science. The Royal Society of Chemistry, Cambridge, UK. 394–406.

Schmitz, K. S. 1990. An Introduction to Dynamic Light Scattering by Macromolecules. Academic Press, San Diego.

Schuck, P. 1998. Sedimentation analysis of noninteracting and self-associating solutes using numerical solutions to the Lamm equation. *Biophys. J.* 75:1503–1512.

Schuck, P., and B. Demeler. 1999. Direct sedimentation analysis of interference optical data in analytical ultracentrifugation. *Biophys. J.* 76: 2288–2296.

Svedberg, T., and K. O. Pederson. 1940. The Ultracentrifuge. Oxford University Press, London.

Tanford, C. 1961. Physical Chemistry of Macromolecules. Wiley, New York.

Tardieu, A., A. Le Verge, M. Malfois, F. Bonneté, S. Finet, M. Riès-Kautt, and L. Belloni. 1999. Proteins in solution: from x-ray scattering intensities to interaction potentials. *J. Crystal Growth.* 196:193–203.

van Holde, K. E., and W. O. Weischet. 1978. Boundary analysis of sedimentation velocity experiments with monodisperse and paucidisperse solutes. *Biopolymers.* 17:1387–1403.

Wills, P. R., L. W. Nichol, and R. J. Siezen. 1980. The indefinite self-association of lysozyme: consideration of composition-dependent activity coefficients. *Biophys. Chem.* 11:71–82.

Winzor, D. J., and P. R. Wills. 1994. Omega analysis and the characterization of solute self-association. *In* Modern Analytical Ultracentrifugation. Birkhäuser, Boston. 66–80.